Journal of Physics: Conference Series **640** (2015) 012008 doi:10.1088/1742-6596/640/1/012008

Aggregation process of Aβ_{1-40} with non-Aβ amyloid component of α-synuclein

Cindie Eugene, Normand Mousseau

Département de Physique and Groupe de recherche sur les protéines membranaires (GEPROM), Université de Montréal, C.P. 6128, succursale Centre-ville, Montréal (Québec), Canada

E-mail: normand.mousseau@umontreal.ca

Abstract. Many neurodegenerative diseases, such as Alzheimer's and Parkinson's diseases, are characterized by the presence of amyloid fibers. Recently, attention has turned from the fibers to the early stages of oligomerization where toxicity could be highest. Here, we focus on the interactions between non-Aβ amyloid component of α-synuclein (NAC) and Aβ_{1-40}, two proteins found in amyloid fibrils associated with Alzheimer's disease. We combine the coarse-grained OPEP potential with a Hamiltonian and temperature replica exchange molecular dynamics simulation (HT-REMD) to identify mechanisms leading to the formation of secondary structures promoting fibrillation. We observe that the propensity to form beta-sheet remains the same for Aβ_{1-40} whereas is decreases significantly for NAC. In particular, the 25-35 region of Aβ_{1-40} is a significant area of secondary structure stabilization with NAC. The ionic interactions between salt-bridge D23 and K28 in Aβ_{1-40} and K20 and E23 in NAC of the heterogeneous dimer are consistent with the salt-bridges found in NAC and Aβ_{1-40} homogenous dimers and allow us to see that these interactions don't necessarily dominate the interchain stabilizations. Our numerical simulation also show the formation of interaction between the early oligomer of NAC and Aβ_{1-40}.

1. Introduction

Amyloid proteins are known for their implications in many neurodegenerative diseases [1, 2]. While research focus was initially on large amyloid fibrils, first associated with the various diseases, attention has turned, over the last decade, to small metastable aggregates believed to be the main toxic agent [3, 4]. In spite of considerable experimental efforts, these structures remain difficult to characterize due to their metastability and a very rich energy landscape leading computer simulations to play a major role to fill some of the knowledge gap regarding these systems (for a recent review of the problem see, for example, Ref. [5]).

Alzheimer's disease is one of the prototypical amyloid diseases and, has such, it has received considerable attention. Experimentally and numerically, for example, the aggregation of full length β-amyloid (Aβ), associated with this diseases, and related fragments has been at the center of efforts for understanding the onset of amyloid aggregation. The interest for this protein is due, in part, to the richness of *in vivo* Aβ aggregation, which is associated with a range of cleaved lengths ranging from 39 to 43 residues, even though two lengths dominate [6]: Aβ_{1-40} and A β_{1-42}. Onset of aggregation studies have therefore been mostly done with the former sequence, the dominant component of amyloid fibrils, which shows a slower and easier to control aggregation mechanism.


Content from this work may be used under the terms of the Creative Commons Attribution 3.0 licence. Any further distribution of this work must maintain attribution to the author(s) and the title of the work, journal citation and DOI.
Published under licence by IOP Publishing Ltd

In addition to Aβ, however, it has been known for 20 years that a second protein is present in amyloid fibrils associated with Alzheimer's disease: the non-amyloid component (NAC), a 35-residue fragment corresponding to α-synclein's strongly hydrophobic central region, a protein that is also a major component of Lewy bodies and neurites associated with Parkinson's disease but is also found in the brain of 60 % of Alzheimers disease patients. [7, 8, 9].

Relatively little attention has been given to the NAC and its interaction with Aβ, both experimentally and numerically, over the last years. [10, 11] This is due, in part, to the already difficult task of characterizing the role of Aβ alone and because the full α-synuclein protein is, in itself, an amyloid protein associated with a major degenerative disease.

Nevertheless, there are a number of reasons to look in more details into NAC aggregation mechanisms and its relation to Aβ's aggregation. First, toxic oligomers share some common structural properties that have yet to be identified and can only be resolved by comparing the oligomerization process of as many sequences as possible, since most turn out to be very difficult to characterize experimentally and computationally; a recent study of the NAC monomer, dimer and trimer confirms the computational interest of this sequence for the study of the onset of aggregation [12]. Second, most studies of heterogeneous aggregation have focused on various length or mutated Aβ-sequences. Looking at the interactions between NAC and Aβ offers a more complex but still manageable system to study this question. Finally, recent experimental evidence show evidence that α-synuclein increases Aβ's toxicity, although the mechanism is still unclear. [13, 10]

In this article, we focus on the first steps in the formation of heterogenous oligomers of Aβ_{1-40} and NAC using replica-exchange molecular dynamics (REMD) coupled with the coarse-grained OPEP potential.[14, 15, 16] This setup was already used successfully to characterize NAC's onset of homogeneous oligomerization [12]. More precisely, we look at the evolution taking place in the three-dimensional structures of Aβ_{1-40} monomer and dimer with NAC monomer to speculate on the role of stabilizer accelerating the onset of beta-sheet organized structure earlier in the polymerization mechanism. We find that these two sequences do associate to form interconnected β-rich structures, with an interaction that supports Paik and al. [17] experimental results regarding the role of Aβ's 25-35 region in coupling with the NAC peptide, and lead to enhanced β-sheet formations that is also observed with the NAC + Aβ dimer system.

2. Methods

We simulate the structural and thermodynamical properties of small amyloid aggregates composed of a α-synuclein non-Aβ amyloid component (NAC) monomer coupled with Aβ_{1-40} monomer or dimer. The amino acid sequence of the 37-residue NAC and Aβ_{1-40} are given by EQVTNVGGAVVTGVTAVAQKTVEGAGSIAAATGFV and DAEFRHDSGYEVHHQ-KLVFFAEDVGSNKGAIIGLMVGGVV respectively. Intra and interpeptide interactions are described with the coarse-grained Optimized Potential for Efficient peptide structure Prediction (OPEP) version 3.2. This potential focuses on the heavy backbone atoms, reducing the amino acid representation to six beads: Cα, N, H, C, and O and one bead for the side chain except for the proline amino acid which is represented by all heavy atoms [18].

The propensities of each residue to adopt α and β conformations are taken into account through four-body hydrogen bonding terms. These generic terms are essential to stabilize the appropriate secondary structure with having successfully been applied to a number of systems including many amyloid-forming proteins such as polyglutamine [19], amylin [20, 14] and various segments of Aβ [21, 22, 23, 24, 25, 26, 27].

Following our previous work on NAC oligomers [12], simulations are performed using the Hamiltonian-temperature replica exchange molecular dynamics, [19, 14, 26] HT-REMD, a hybrid of temperature replica exchange (T-REMD) and Hamiltonian replica exchange (H-REMD) is combined with OPEP. For the system studied here, we launch a total of 40 replicas: 35

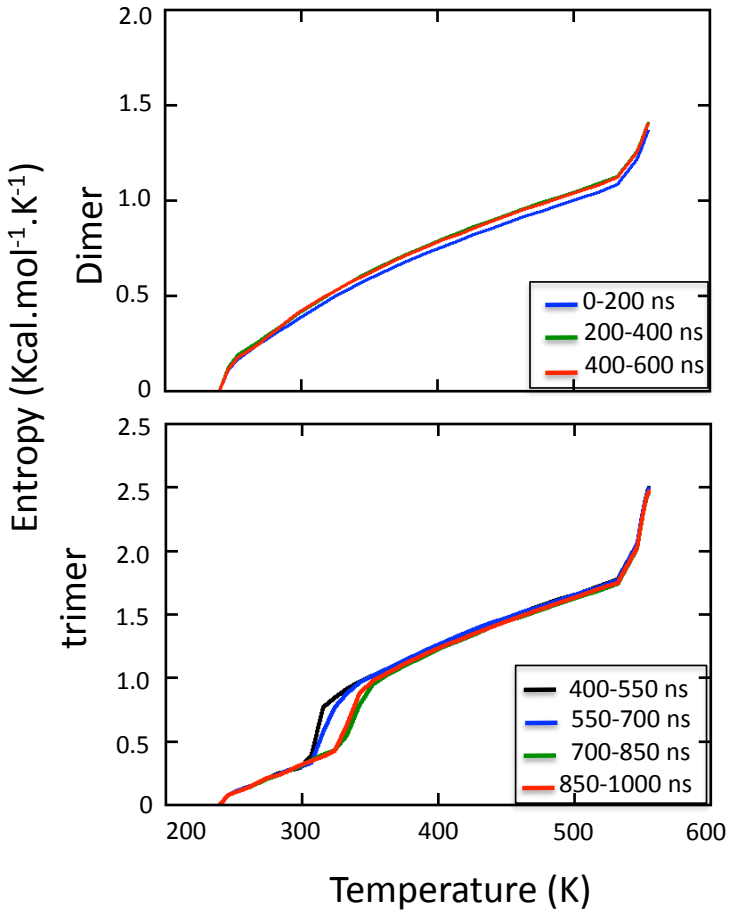

Figure 1. Entropy as a function of temperature taken over three subsequent 200-ns time intervals for the NAC and Aβ_{1-40} system and the NAC plus 2 Aβ_{1-40} systems. Equilibrium is reached after the first 200 ns for the two-chain system and after 700 ns for the three-chain one. Statistical error (not shown for legibility) is about $\pm$0.01 kcal/(mol*K)

replicas are launched at temperatures ranging from 240 to 555 K and distributed according to a logarithmic scale while the remaining 5 replicas are launched, at the highest temperature, with reduced non-bonded attractive forces corresponding to 0.8, 0.7, 0.6, 0.4 and 0.2 of the initial interaction.

Newton's equations of motion are integrated with a 1.5 fs timesteps with the hydrogen high-frequency vibrations stabilized by the Rattle algorithm timesteps [28]. The temperature is controlled with the Berendsen thermostat using an external coupling constant of 100 fs [29]. Replica exchanges are attempted every 7.5 ps. The dimeric system composed of the monomer NAC of α-synuclein and Aβ_{1-40} is simulated for 700 ns per replica (total 28 μs) in a 40 Å-radius sphere with reflecting boundary conditions. The trimeric system, one NAC and two Aβ_{1-40} chains, is run for 1000 ns per replica, for a total of 40 μs.

The replica-exchanged adapted weighted histogram method, PTWHAM [30], is used for the reconstruction of the thermodynamical properties of the oligomer. STRIDE, a protein secondary

structure assignment code based on the combined use of hydrogen bond energy and statistically derived backbone tortional angle informations [31], is selected to predict the secondary and tertiary structures. For clustering we use the Cα root-mean square deviations (rmsd) and follow Daura's procedure [32]: we first identify the largest cluster with a rmsd of 2.5 Å; all configurations belonging to this cluster and then removed and the procedure is repeated to identify the second and following clusters.

The entropy, obtained from the free energy computed with PTWHAM, is used to determine when the system's convergence as it is a direct measure of the number of visited configurations. To estimate convergence, we compute the entropy over a non-overlapping sequence of time intervals and consider that equilibrium is reached when the entropy, computed over the whole temperature range, becomes constant. As seen in Fig. 1, the entropy converges after 200 ns/replica for the NAC+Aβ dimer. For the NAC+ 2 Aβ, we observe a jump in in the entropy near room temperature, as discussed below, this is caused by the dissociation into a monomeric NAC with a dimeric Aβ in most of replicas. Some results are presented here, however, but they must be confirmed by further simulation. We present results at 350 K, to avoid the problematic region found between 300 and 340 K, and will focus mostly on the NAC+Aβ. Statistical error bars are evaluated using the bootstrapping algorithm. [33]

3. Results

Table 1. Percentage of secondary structure taken at 300 K for the dimer NAC+Aβ and 350K for the trimer NAC+ 2Aβ . Results for the dimer and the trimer are averaged over their interval of convergence (see Section 2). Statistical error is estimated at ±1% but see the methodology for a discussion regarding the trimer.

Sec. struct. (%)	Dimer		Trimer	
	per species	average	per species	average
α-helix	11 (NAC) - <1(Aβ_{1-40})	6	27 (NAC)- <1(Aβ_{1-40})	14
β-strand	8 (NAC) - 9 (Aβ_{1-40})	9	<1 (NAC)- 29 (Aβ_{1-40})	14
Turn	58 (NAC) - 53 (Aβ_{1-40})	56	46 (NAC) - 27 (Aβ_{1-40})	37
Random coil	23 (NAC) - 38 (Aβ_{1-40})	31	26(NAC) - 43 (Aβ_{1-40})	35

We first present the detailed results for the two systems under study: a heterogeneous dimeric compound formed of a NAC and a Aβ_{1-40} monomers and a heterogeneous trimeric compound formed of one NAC and two Aβ_{1-40} monomers. In the two cases, we first place fully stretched peptides at random in the box and first relax the configuration at zero Kelvin. Configurations are then thermalized at the various temperatures used in the replica-exchange molecular dynamics and the run is started.

3.1. The dimer of Aβ_{1-40} with non-Aβ amyloid component of α-synuclein

We simulated the dimer for 700 ns per replica and collected the last 500 ns for analysis. In this interval, we find relatively little overall secondary structure : α-helix propensity is about 6 % while β-stand propensity is 50 % higher, at 9% (Table 1). As shown in Fig. 2, α-helices are concentrated in the NAC chain (with a 11 % propensity), with two peaks at residues Q2-T12 and G13-A29 showing a ∼22% and ∼30% propensity, respectively. We also observe a small helical tendency at residues 56-63 (A21-G28 in Aβ_{1-40}) with a propensity of ∼6%, for an overall α-helical propensity of only 1%.

β-strands are slightly more common overall with no dominating region: the highest per-residue propensity barely reaches 25 %. In NAC, two regions dominate at residues Q2-T12 and

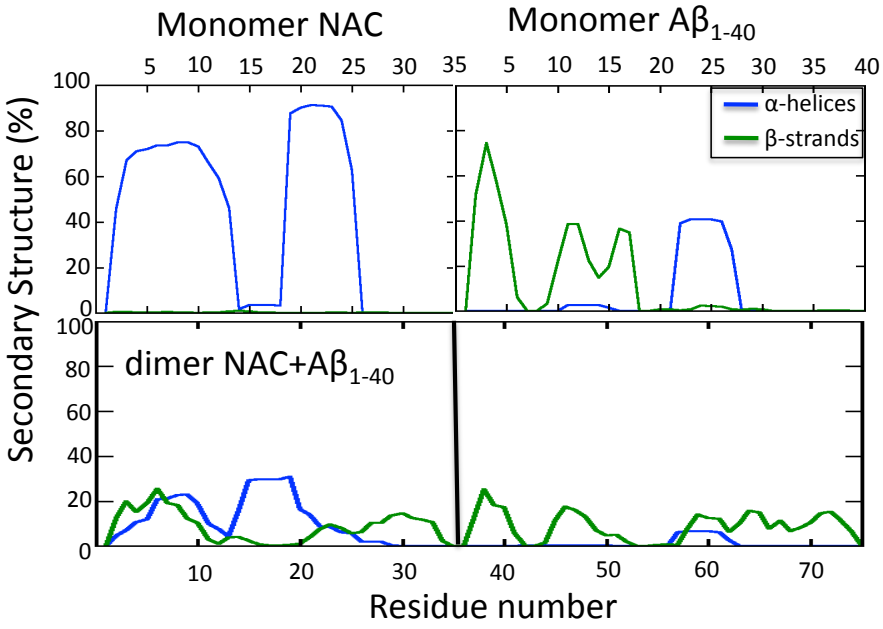

Figure 2. Top: α-helix and β-strand propensity as a function of residue number at 300K for isolated NAC and Aβ monomers (taken, respectively, from Refs. [12] and [26]). Bottom: α-helix and β-strand propensity for the NAC/Aβ dimer calculated over the 200-700 ns time interval.

K20-F34 with probabilities of about 25 and 14 %, respectively for a total β-strand propensity of 9 %, slightly less than for α-helices.

Aβ shows, for its part, three regions with non-zero probability of forming β-sheets: residues A2-D7 (37-42 in Fig. 2), S8-H18 (43-53) and D23-V40 (58-75) of Aβ_{40}, with a maximum propensity per residue of $\sim$25%, $\sim$17% and 15%, respectively. From Table 1, we note that the total β-strand propensity of Aβ_{40} is at 9%, small but much higher than the α-helical propensity.

Maps showing total, intrachain and interchain contacts are presented in Fig. 3. Here again, we observe a wide distribution of contacts, both interchain and interchain. While most of these contacts occur with a probability below 50 %, a number of long-range interchain interactions are present in a majority of structures. We note, in particular, V10-I66 (I31 in Aβ's sequence) and V17-V53 (V18) and V35-F54 (F19) (respectively with $\sim$65% for the first and second and $\sim$80% for the third interaction).

The relatively small probability of forming well-defined contacts and secondary structure elements is explained by the diversity of tertiary structures that are visited by dimer. Figure 4 shows the six dominant clusters that represent, together, only about 30 % of all configurations, as defined with a 2.5 Å-RMSD cut-off. These six clusters show a very diverse set of secondary and tertiary elements that we describe below in some details.

D1, the first cluster, with an occurrence of 8.7 %, shows no β-strand or α-helical secondary structure. However, it displays many interchain contacts responsible for maintaining the tertiary structure in a mostly antiparallel arrangement (see Fig. 5). D2, that represents 4.7 % of all visited structures, is more structured. It forms a short anti-parallel interchain β-sheet, composed of residues N5-V6 of NAC and A2-E3 of Aβ_{1-40}. We also see an α-helix in the region 14-20. Looking at contacts (Fig. 5), we observe that the few interchains contacts are dominated, beside the β-sheet, by residues V6 of NAC and F4 of Aβ (F39 in the figures).

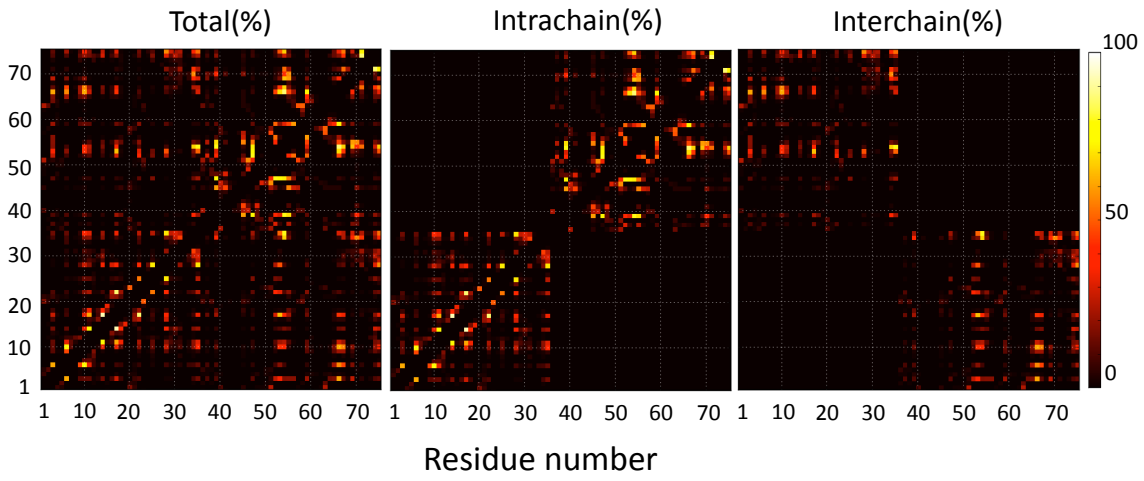

Figure 3. Map of the contact propensity of total, intrachain and interchain contacts the NAC/Aβ_{1-40} dimer. The NAC runs from residues 1 to 35 and Aβ from residues 36 to 75 over the 200-700 ns time interval. The total contact propensity is calculated from the intrachain and interchain contacts.

D3, with a formation probability of 4.6 %, shows a 3-stranded intrachain antiparallel β-sheets at residues E3-R5/E11-H14/V24-D26 in Aβ_{1-40}, with few interchain contacts. D4, representing 3,9 % of all visited configurations, also forms a short antiparallel interchain β-sheet, like D2, but between NAC's Q2-V3 and Aβ's D23-V24. It also forms an α-helix in NAC between residues V6 and A9. Looking at contacts (Fig. 5), we note that residues I31 and I32 in Aβ_{1-40} have a high propensity to form interchain contacts with some regions of NAC: the region V3-V6 and V10-V14 and F34-V35. Residues I31 and I32 are important in the interchain stabilization of the structure.

D5, that occurs 3.5 % of the time, is the only structure with both an intrachain and an interchain β-sheet. The antiparallel interchain β-sheet is found between residues T4-G8 of NAC and K28-I32 of Aβ. A short intrachain antiparallel sheet is also observed at residues A2-E3/Q16-K17 of Aβ. D6, finally, with an occurrence probability of 3.5 %, shows, like for D3 and D4, relatively few interchain contacts, with the exception of an antiparallel region between residues V17-V22 of NAC and L17-E22 of Aβ. D6 is also rich in secondary structure with an intrachain antiparallel β-sheet formed by NAC's residues G7-V10 and A29-T32, as well as a short α-helix at residues E11-H13 of Aβ.

In terms of salt-bridges, while the intramolecular bridge at K20-E23 is present on NAC for all dominant clusters, we also observe a contact between E11-K16, K16-E22, E22-K28 and D23-K28 of Aβ_{1-40}) with a percentage close to 80 in a majority of the six clusters, suggesting that these few charged residues, particularly K16 and E22 (51 and 57 in the total sequence) play an important role for stabilize intrachain structures. There are no interchain salt-bridges.

3.2. The trimer : two Aβ_{1-40} and a non-Aβ amyloid component of α-synuclein peptides

We also simulated a trimer composed of two Aβ_{1-40} and one NAC peptides for 1000 ns per replica and collected the last 300 ns for analysis. While the entropy is relatively stable over this time range, we find that most replicas sampled a decomposed system with an isolated NAC monomer and a Aβ_{1-40} dimer. Properties for the full configurational ensemble are given in Table 1, where we note the same amount of secondary structure: α-helix and β-stand propensity, at 14%.

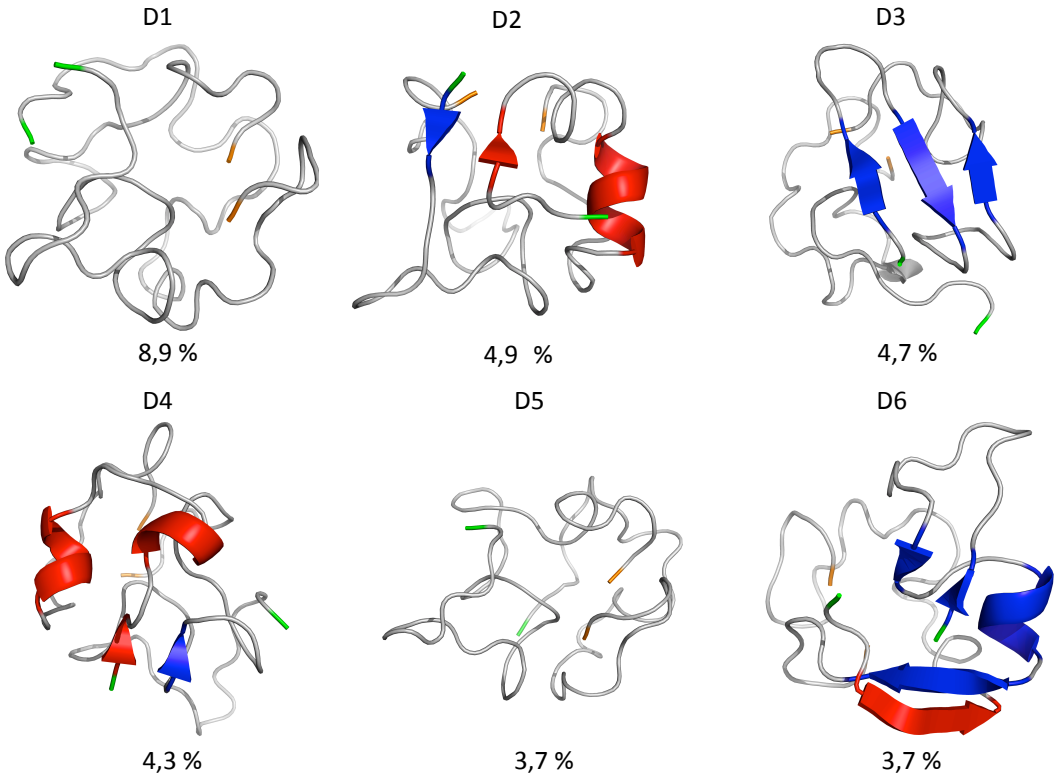

Figure 4. Dominant clusters' centers for the dimer NAC/Aβ_{1-40} averaged over the 200-700 ns time interval. The N-terminal and the C-terminal are shown in green and orange, respectively. The NAC chain is shown in red, Aβ_{1-40} in blue.

α-helices are concentrated in the NAC chain and β-stand in Aβ_{1-40}.

A few replicas produce a bound trimer however. The dominant cluster for these runs, that represent only 7 % of all configurations, and defined with a 3 Å-RMSD cut-off is presented in Fig.6. This cluster show a interchain contact β-stand, between residue A31-G33 (NAC) /V36-G38(Aβ_{1-40}) and A30-G33(NAC)/V36-V39(Aβ_{1-40}).

Clearly, while these results show that interactions between the two species are possible among larger aggregates, further simulations are necessary to evaluate whether or not the dislocated structure is due to the initial setting and the fact that OPEP's relatively short cutoff prevents peptides, once far from each other, to attract, or is characteristic of an important part of the configurational space of this setup.

4. Discussion

As discussed above, the NAC represents about a 10 % of the proteins found in amyloid fibrils associated with Alzheimer's disease. [7] Its role in aggregation and toxicity remains to be understood and it is not clear whether it is simply a contaminant or whether it impacts the fibril growth. This impact could be multiple. It could help stabilize the Aβ monomers or

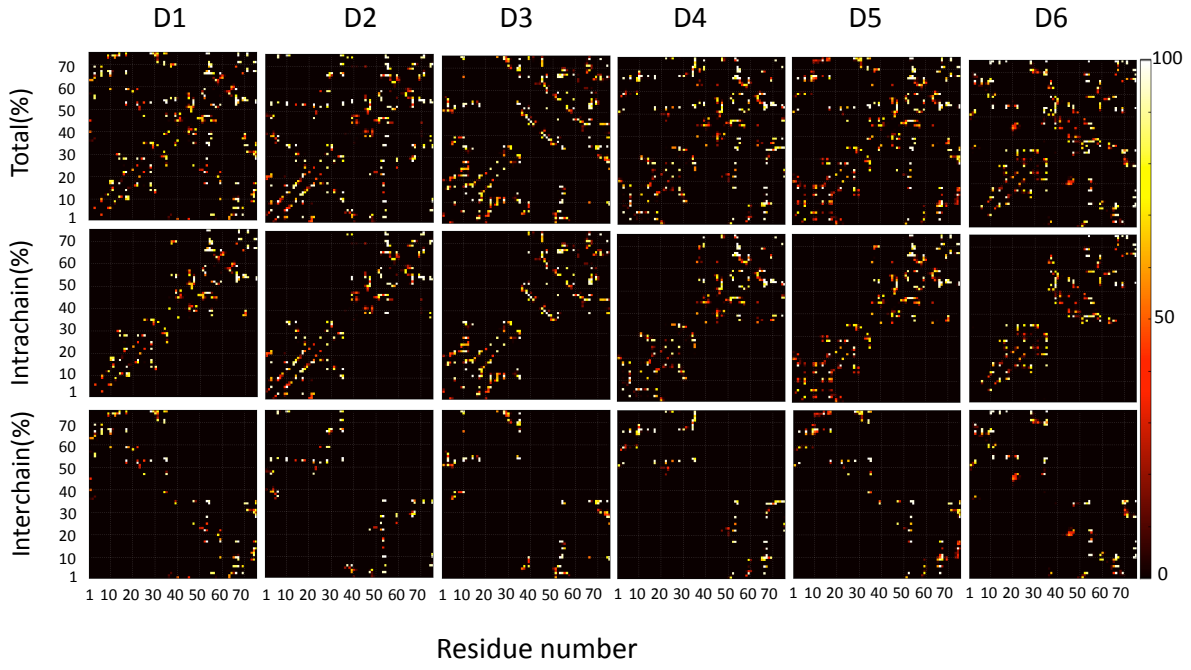

Figure 5. Map of the total, intrachain and interchain contact propensity for the six dominant clusters in the mixed dimer. The NAC runs from residues 1 to 35 and Aβ from residues 36 to 75. The total contact propensity is calculated by summing the intrachain and interchain contacts.

oligomers as they grow into fibril or play a more active role into the oligomeric structures.

There exists very few experimental papers that attempt to characterize the interaction between the NAC and Aβ. Indeed, amyloid oligomers are particularly difficult to control and, even for simply monospecies oligomers, very little precise structural information exists on the structure of the dimer or small assemblies.

In *in vitro* growth studies, Han *et al.* explored the nucleation dependent polymerization mechanism between NAC and Aβ_{1-40}. [34] They show, first, that the NAC peptide does aggregate into amyloid fibrils. Han *et al.*, moreover, demonstrate that NAC fibrils can seed Aβ fibrils' formation and, *vice-versa*, that Aβ fibrils can seed NAC amyloid aggregation. While this heterogeneous seeding is possible, it remains less efficient than homogeneous seeding as determined by the lag time before fibril growth takes place, suggesting that the structural match between these two sequences is less amyloid prone that with a pure system. [34] While this work supports a positive interaction between NAC and Aβ leading to amyloid formation, it is not clear whether or not the two chains can interact at the monomeric level or only through preformed fibril structures. Indeed, Han *et al.* find no evidence of an increase in the formation of insoluble aggregates in mixed NAC and Aβ solutions compared with pure ones. In some cases, the rate is even slowed down, although this results says nothing about the formation of soluble oligomers and their relative toxicity. The first part of the question is partially answered by Paik *et al.* in an experiment on the self-oligomerization of the full-length α-synuclein with Aβ_{25-35} [17]. Paik and collaborators confirm that the 25-35 region of the Aβ is sufficient for promoting α-synuclein aggregation. They also show that, although Aβ_{25-35} could interact with other regions of α-synuclein, the NAC region seems to be a preferred binding site. Repeating their experiments with a reverse 35-25 sequence, Paik *et al.* showed that the orientation was essential for promoting oligomerization [17].

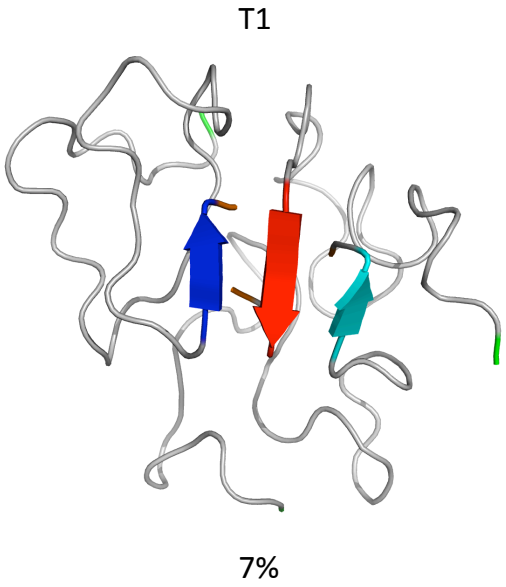

Figure 6. The dominant cluster's center for the aggregated trimer NAC+ 2 Aβ_{1-40} over the 700-1000 ns time interval. The N-terminal and the C-terminal are shown in green and orange, respectively. The NAC chain is shown in red, the Aβ_{1-40} in dark and light blue.

Our simulations, that show binding of both peptides, are compatible with these observations. For example, Fig. 3 shows that contacts between Aβ and NAC are dominated by residues V17(NAC) with V53(Aβ's V18) and V35(NAC) with F54(Aβ's F19), showing that, indeed, Aβ's N-terminal is relatively inactive here. Moreover, interchain β-sheets involve residues in this region : D3(24-26), D4(23-24), D5(28-32) and D6(26-32). These results confirm the interaction and the co-stabilization of secondary structure in or around region 25-35 of Aβ and NAC.

Comparison between our results and the formation of pure NAC and Aβ dimers allows us to link our simulations to Han *et al.* results. Côté *et al.* studied the assembly of Aβ_{1-40}, Aβ_{1-40}(D23N) and Aβ_{1-42} dimers using the same OPEP and HT-REMD methodology, allowing a direct comparison with results presented here. [16] They show that while β-strand propensity increase comparing with the monomer, particularly at the fibril-loop region(22-28) and C-terminal(29-40), the overall change in secondary structure remains small for Aβ_{1-40}: α-helical propensity goes from 6 to 1.3 % while β-strand propensity moves form 12 to 13 %, similar to what is observed here. For the NAC peptide, however, the difference is more important: while the β-sheet content reaches 24 % for the NAC dimer, it is only 9 % here.

Moreover, if the propensity is lower, β-sheets observed in the heterogeneous dimer are similar to those observed in the homogenous dimers, with a relatively high β-sheet propensity in the N-terminal for Aβ and at the N-terminal and C-terminal for NAC, even though some of these β-sheets are formed by the two chains. We also observe an important presence for the salt-bridge between D23 and K28 of Aβ_{1-40}, and K20-E23 is present on NAC, in agreement with Côté *et al.* results. [26, 16] and our study of NAC dimer.

5. Conclusion

In this study, we simulated the dimer and trimer of $A\beta_{1-40}$ with non-$A\beta$ amyloid component of α-synuclein. We focused on this system in order to understand the possible role of NAC in the amyloid fibrils associated with Alzheimer's disease, for which $A\beta_{1-40}$ is the major component. Our simulations confirm experimental observations by Paik *et al.*[17] that the 25-35 region is a significant area of secondary structure stabilization for the dimer with NAC. Comparing with NAC and $A\beta$ previous study using the same simulation and analysis procedure, we find the beta-sheet propensity remains the same for $A\beta_{1-40}$ and decrease for NAC. The same ionic interaction between D23-K28 in $A\beta_{1-40}$ and K20-E23 in NAC in the homogenous oligomer are found in heterogenous and confirm ionic interaction is not involve in the interchain stabilization.

Clearly, more similations and experiments are needed to establish the full interaction between NAC and $A\beta$. Our results, however, confirm that NAC could be used as one of the numerical standards for studying protein aggregation both in a pure and a mixed form.

6. Acknowledgments

This work is supported in part by the Natural Science and Engineering Research Council of Canada, the Canada Research Chair Foundation and the Fonds de recherche du Québec - Santé. This work was made possible through generous allocation of computer time by Calcul Québec/Compute Canada.

References

[1] Ross C and Poirier M 2004 *Nature medicine* **10 Suppl** S10–7
[2] Ross C and Poirier M 2005 *Nature reviews. Molecular cell biology* **6** 891–8
[3] Bodles A, Guthrie D, Greer B and Irvine G 2001 *Journal of neurochemistry* **78** 384–395
[4] Taylor J, Hardy J and Fischbeck K 2002 *Science (New York, N.Y.)* **296** 1991–1995
[5] Derreumaux P (ed) 2013 *Alzheimer's disease: Insights into Low Molecular Weight and Cytotoxic Aggregates from In Vitro and Computer Experiments* (Imperial College Press)
[6] Haass C and Selkoe D J 2007 *Nat. Rev. Mol. Cell Biol.* **8** 101–112
[7] Uéda K, Fukushima H, Masliah E, Xia Y, Iwai A, Yoshimoto M, Otero D A, Kondo J, Ihara Y and Saitoh T 1993 *Proc Natl Acad Sci U S A* **90** 11282–6
[8] Duda J, Lee V and Trojanowski J 2000 *Journal of neuroscience research* **127** 121–127
[9] Mikolaenko I, Pletnikova O, Kawas C H, O'Brien R, Resnick S M, Crain B and Troncoso J C 2005 *J Neuropathol Exp Neurol* **64** 156–62
[10] Kazmierczak A, Strosznajder J B and Adamczyk A 2008 *Neurochem Int* **53** 263–9
[11] Kazmierczak A, Czapski G A, Adamczyk A, Gajkowska B and Strosznajder J B 2011 *Neurochem Int* **58** 206–14
[12] Eugène C, Laghaei R and Mousseau N 2014 *J. Chem. Phys.* **141** 135103
[13] Mandal P K, Pettegrew J W, Masliah E, Hamilton R L and Mandal R 2006 *Neurochem Res* **31** 1153–62
[14] Laghaei R, Mousseau N and Wei G 2011 *J. Phys. Chem. B* **115** 3146–3154
[15] Liang G, Zhao J, Yu X and Zheng J 2013 *Biochemistry* **52** 1089–100
[16] Côté S, Laghaei R, Derreumaux P and Mousseau N 2012 *J. Phys. Chem. B* **116** 4043–4055
[17] Paik S, Lee J H, Kim D H, Chang C S and Kim Y S 1998 *FEBS 19685* **421** 73–76
[18] Maupetit J, Tuffery P and Derreumaux P 2007 *Proteins : Struct., Funct., Bioinf.* **69** 394–408
[19] Laghaei R, Mousseau N and Wei G 2010 *J. Phys. Chem. B* **114** 7071–7077
[20] Laghaei R and Mousseau N 2010 *J. Chem. Phys.* **132** 165102
[21] Chen W, Mousseau N and Derreumaux P 2006 *J. Chem. Phys.* **125** 84911
[22] Wei G, Mousseau N and Derreumaux P 2007 *Prion* **1** 3–8
[23] Dong X, Chen W, Mousseau N and Derreumaux P 2008 *J. Chem. Phys.* **128** 125108
[24] Chebaro Y, Mousseau N and Derreumaux P 2009 *J. Phys. Chem. B* **113** 7668–7675
[25] Melquiond A, Dong X, Mousseau N and Derreumaux P 2008 *Curr. Alzheimer Res.* **5** 244–250
[26] Côté S, Derreumaux P and Mousseau N 2011 *J. Chem. Theory Comput.* **7** 2584–2592
[27] Lu Y, Wei G and Derreumaux P 2011 *J. Phys. Chem. B* **115** 1282–1288
[28] Andersen H 1983 *J. Comput. Phys.* **52** 24–34
[29] Berendsen H, Postma J, van Gunsteren W, DiNola A and Haak J 1984 *J. Chem. Phys.* **81** 3684–3690
[30] Chodera J, Swope W, Pitera J, Seok C and Dill K 2007 *J. Chem. Theory Comput.* **3** 26–41

[31] Frishman D and Argos P 1995 *Proteins: Struct., Funct., Genet.* **23** 566–579
[32] Daura X, Suter R and van Gunsteren WF 1999 *J. Chem. Phys.* **110** 3049–3055
[33] Newman M E J and Barkema G T 1999 *Monte Carlo Methods in Statistical Physics.* (Clarendon Press (Oxford))
[34] Han H, Weinreb P H and Lansbury P T 1995 *Chemistry & biology* **2** 163–169